Diffusion at the interface of laser welded polyamide-6.6 and aluminum assemblies

Hirchenhahn, P.; Al-Sayyad, A.; Bardon, J.; Plapper, P.; Houssiau, L.

Published in:
Journal of Materials Research and Technology

DOI:
10.1016/j.jmrt.2024.11.092

Publication date:
2024

Document Version
Publisher's PDF, also known as Version of record

Journal of Materials Research and Technology 33 (2024) 7303–7309

Contents lists available at ScienceDirect

Journal of Materials Research and Technology

journal homepage: www.elsevier.com/locate/jmrt

Diffusion at the interface of laser welded polyamide-6.6 and aluminum assemblies

P. Hirchenhahn [a], A. Al-Sayyad [b], J. Bardon [c], P. Plapper [b,1], L. Houssiau [a,*]

[a] LISE, Namur Institute for Structured Materials (NISM), Université de Namur, rue de Bruxelles, 61 5000, Belgium
[b] Research Unit in Engineering Science, Université de Luxembourg, 6 rue de Coudenhove-Kalergi, L-1359, Luxembourg
[c] Luxembourg Institute of Science and Technology, 5 avenue des Hauts-Fourneaux, L-4362, Esch-sur-Alzette, Luxembourg

ARTICLE INFO

Handling editor: L Murr

Keywords:
Diffusion
Interface
Laser welding
ToF-SIMS
Information entropy

ABSTRACT

Polymer/metal assemblies are widely used in industry, especially the automotive industry, to get more cost efficient and light weight structures. Although they present many advantages, their assembly remains challenging. Laser welding is an effective solution. Indeed, it is fast, presents high design freedom, and does not require any interstitial material. Furthermore, surface pretreatment can tune mechanical resistance. However, the root causes of adhesion remain partly unknown. The existence of chemical bonding at the interface has already been established, but other adhesion phenomena, such as diffusion, remain to be investigated. The aim of this study is to investigate the existence of diffusion at the interface between the polymer and the metal after laser welding. Therefore, a common material combination was used: polyamide-6.6 and aluminum. A thin film of polyamide-6.6 was deposited on mirror-polished aluminum, and two depth profiles out and in the weld were acquired by ToF-SIMS and compared. The results show that the diffusion of aluminum occurs at the interface of polyamide-6.6, with a diffusion length of approximately 22 nm.

1. Introduction

The applications of hybrid polymer-metal assemblies are numerous in many different fields, such as the automotive industry, for lightweight structures, or in the biomedical industry, for implants for instance. Nevertheless, the major issue still remains to assemble the two materials. Three main ways of assembling exist: (1) mechanical fastening [1], (2) adhesive bonding [2,3], and (3) welding [4–7]. For automotive applications, the weight increase induced by the mechanical fastening is not complying with lightweight structures responding to ecological issues. For biomedical applications, the low corrosion and wear resistance of mechanical assemblies exclude this possibility. Adhesive bonding is not a universal solution, as generally good adhesives are generally harmful chemicals and present low biocompatibility. In addition, the application of adhesive bonding needs several expensive and time-consuming preparation and post-treatment steps. In this context, the application of welding techniques appears to be a strong solution.

There is a high variety of welding techniques, but one in particular is catching attention: laser welding. Laser welding offers many advantages addressing the different issues found in mechanical fastening and adhesive bonding [4–8]. The technique does not require any interstitial materials nor any pre- or post-treatment, making the assembling even faster than it already is. But the use of pretreatments can be beneficial to tune the mechanical resistance [8–11]. The design of the pieces is only limited by the possibility to shine the laser at the desired place, giving a huge design freedom in the shape and the size of the assemblies. The only disadvantage found is its initial cost of implementation in a production line [4–8].

The principle of laser welding is quite simple. A laser is irradiated on one of the materials to be assembled. The laser beam is absorbed, generating heat, which will allow to weld the pieces together. Two main configurations for laser welding are studied: (1) direct [8,12,13] and (2) indirect [8,11,13] laser welding. In direct laser welding, the laser beam is irradiated through the polymer to the interface, but this configuration limits the number of polymers that can be welded, as the polymer must be transparent to the laser beam used. In indirect welding, the laser beam is irradiated on the metal, and the heat diffuses to the metal-polymer interface. This allows a larger choice of materials to be welded [4–8]. The developments in laser welding are focused mainly on new materials combinations [12,14–19] or on surface pretreatment

* Corresponding author
E-mail address: laurent.houssiau@unamur.be (L. Houssiau).
[1] in memoriam.

https://doi.org/10.1016/j.jmrt.2024.11.092
Received 30 July 2024; Received in revised form 8 November 2024; Accepted 9 November 2024
Available online 14 November 2024

prior to welding as already mentioned [8,10,20,21]. Nonetheless, the root causes of adhesion are still not well understood. The adhesion theory is composed of four phenomena: mechanical interlocking [22], chemical and physical bonding [23], diffusion [24,25], and electrostatic interactions [26]. Mechanical interlocking is known to play a role in laser welding adhesion [8,27]. In 2009, Georgiev et al. [28], investigated chemical bonding between laser welded Teflon and titanium. More recently, Hirchenhahn et al. [29–31] investigated the formation of chemical bonds at the interface of aluminum/polyamide-6.6 and titanium/polyamide-6.6 assemblies and described also the formation mechanism. Electrostatic interactions [32] are experimentally difficult to study, and generally considered as secondary adhesion effects. To the best of our knowledge, a diffusion phenomenon between laser welded hybrid assemblies has never been reported. The goal of the present work is to investigate the existence of such a phenomenon and characterize it. In this study, two common materials in industry were chosen: polyamide-6.6 for the polymer, and aluminum for the metal.

2. Materials and methods

To study a possible diffusion phenomenon at the interface of aluminum-polyamide-6.6 laser welded assemblies, samples were prepared as following. First, aluminum plates were mirror polished to limit the impact of roughness on the analysis. Second, a thin film of polyamide-6.6 was deposited by spin-coating on the previously mirror polished metal plates. The thickness of the polymer thin film was measured by profilometry. The two materials were laser welded, and finally depth profiles were acquired with ToF-SIMS in and out of the weld for comparison.

2.1. Materials

1 mm thick aluminum sheets of high purity (99.999%) were purchased from Goodfellow (Huntingdon, United Kingdom) and cut to 20 × 20 mm^2 plates. Polyamide-6.6 pellets were purchased by Sigma-Aldrich and used as received. 2,2,2-trifluoroethanol at 99+% purity was purchased by Alfa Aesar (Heysham, United Kingdom) and used without further purification.

2.2. Mirror polishing

The mirror polishing of the aluminum plates was performed using an EcoMet 250 pro from Buehler (Leinfelden-Echterdingen, Germany). First a SiC foil of 1200 grit from Struers (Fellbach, Germany) was used, then diamond pastes DiaDuo-2 from Struers of successively 9, 3 and 1 μm were used. For these steps the rotation speed of the sample holder was of 120 rpm, while the grit had a speed of 40 rpm with a 22 N pressure during 5 min. For each step (each grit and paste), the rotation of the two parts was set in the same rotation direction and in the opposite rotation direction alternatively. At last, a colloidal suspension of silicon of 40 nm OP-S from Struers was used with 22 N pressure, during 3 min, with a speed of 180 rpm for the sample holder and 40 rpm for the grit plate with opposite rotation directions.

Roughness measurements were performed by a KLA Tencor P17 mechanical profilometer. Areas of 80 × 80 μm^2 are scanned and Sa (3D unfiltered average roughness amplitude) parameter value was extracted for each area according to ISO 25178. The polished surface is characterized by an average Sa value of 17.6 nm.

2.3. Spin-coating

A solution of 1 w/w% of polyamide-6.6 in 2,2,2-trifluoroethanol was prepared and then spin-coated on the mirror polished surfaces using a Laurell WS-650-23B spincoater (North Wales, United States). The rotation speed was 1000 rpm during 60 s. Afterwards the samples were dried on a hot plate at 37 °C for 1 h.

2.4. Profilometry–thin film thickness

The polyamide-6.6 coatings were peeled-off locally by means of a rigid polymer tip. Topography measurements, 3 experiments per sample, were performed by an Asylum MFP3D Infinity atomic force microscope (AFM) purchased from Oxford instruments (Halifax, United Kingdom). Measurements were performed in AC air topography (intermittent contact) mode with a AC160 tip from Asylum Research, whose resonance frequency and stiffness are approximately 300 kHz and 26 N/m, respectively. 2D profiles were then extracted from topography maps and thickness evaluation was performed by step height calculation.

2.5. Laser welding

A fiber laser (TruFiber 400 from TRUMPF, Ditzingen Germany) with a wavelength of 1070 nm and a spot diameter of 31 μm was used to perform the laser beam welding. The focus of the laser was set to the interface. The beam followed a circular spatial power modulation (wobble trajectory), with an amplitude a = 0.4 mm, a circular oscillation frequency f_{osc} = 500 Hz and a corresponding velocity of the center of the oscillated laser beam v_f = 40 mm s^{-1}. To avoid polymer degradation during the process the heat input was decreased by applying a temporal power modulation on the laser beam, with a temporal frequency 1/T = 25 kHz, a peak power P = 400 W and a pulse duration T_{pulse} = 35 μs. The procedure was fully described previously [11].

2.6. ToF-SIMS measurement

ToF-SIMS depth-profiles were performed on an ION TOF IV (Iontof Gmbh, Münster Germany) out and in the weld. The profiles were acquired in the negative ion mode using a 500 eV Cs^+ profiling beam of 32.4 nA current and a 25 keV Bi_3^+ analysis beam of 0.45 pA for 20 min in interlaced mode. The raster size of the profiling beam was of 400 × 400 μm^2, while the raster size of the analysis beam was of 200 × 200 μm^2. Charge compensation was performed using an electron flood gun. The mass resolution m/Δm was 3600 as measured on the Al^- peak on the overall profiles. The same calibration peak list (see Table 1) and the same peak list was used (see Table 1 in the supporting information). To establish the peak list, ions characteristic of the polymer were selected along with characteristic ions of the metal. Common contaminations were also checked, and some hybrid ions were also added.

3. Theory and calculations

3.1. Information entropy

The information or Shannon entropy was first introduced in 1948 by C. Shannon [33]. This "entropy" can only be calculated in the case of a transmitted information between a source and a receptor, which fits any characterization technique, where the source is the sample and the receptor the detector. The simplest way to understand this information entropy, is to see it as a measure of the number of bits needed to encode information. In short, the information entropy is a measure of the

Table 1
Calibration list with the deviation in ppm and in m.a.m.u.

Peaks	Mass (a.m.u.)	Out of the weld		Weld	
		Deviation in ppm	Deviation in m.a.m.u.	Deviation in ppm	Deviation in m.a.m.u.
CH^-	13.0086	19.4	0.3	7.4	0.1
OH^-	17.0033	−13.1	−0.2	−7.5	−0.1
C_3^-	36.0001	−12.4	−0.4	−4.5	−0.2
C_5H^-	61.0084	−3.1	−0.2	−6.6	−0.4
C_6^-	72.0025	30.6	2.2	27.5	2.0
$Al_2O_2^-$	85.9535	−20.8	−1.8	−16.7	−1.4
$Al_3O_4^-$	144.9247	1.3	0.2	0.4	0.1

complexity of the transmitted signal. The higher the entropy is, the more bits are needed to transmit the information, the more complex the signal is. This calculus is especially interesting in materials characterization science, as it can help to better understand mixtures or complex samples, to identify different zones. Aoyagi et al. [34]. wrote an extensive article, describing different cases where the information entropy was applied and yielded interesting results in ToF-SIMS, but they also describe the limitations of the information entropy.

Using the Surface Lab software, an automated peak search was done for both profiles (in and out of the weld) in the range from 0 to 1000 m/z with a minimum intensity of 100 counts. As the peak lists obtained for both profiles presented slight differences, they were merged into one and applied to both profiles. This resulted in an automatically generated peak list of 617 peaks.

The information entropy was calculated for both profiles (in and out of the weld) following the same formula as Aoyagi et al. [34] using the automatically generated peak list:

$$S = -\sum_{i=1}^{n} p_i.\ln(p_i) \quad \text{eq. 1}$$

where

$$p_i = \frac{I_i}{I_{total}} \quad \text{eq. 2}$$

I_i is the intensity of the ion i, I_{total} is the total intensity, and n is the number of peaks in the peak list. The calculus was made using an in-house developed Python program.

3.2. Diffusion model

Estimating the diffusion length was made by applying the second Fick law:

$$\frac{\partial C}{\partial t} = D\frac{\partial^2 C}{\partial x^2} \quad \text{eq. 3}$$

where C is the concentration of the diffusing species, aluminum in our case, and D the diffusion constant. The general solution is the following:

$$\frac{C(x;t) - C_0}{C_S - C_0} = 1 - erf\left(\frac{x}{2\sqrt{Dt}}\right) \quad \text{eq. 4}$$

Where C_0 is the bulk concentration and C_s is the surface concentration and $C(x;t)$ is the concentration at a distance x from the surface at time t. Eq. (4) can be modified to:

$$C(x;t) = C_S - (C_S - C_0)erf\left(\frac{x}{2\sqrt{Dt}}\right) \quad \text{eq. 5}$$

The time parameter can be removed, as the system is frozen and no longer evolves. The $2\sqrt{Dt}$ denominator is therefore replaced by a diffusion length k:

$$C(x) = C_S - (C_S - C_0)erf\left(\frac{x}{k}\right) \quad \text{eq. 6}$$

The concentration of aluminum in the polymer before the welding is equal to zero, hence $C_0 = 0$:

$$C(x) = C_S\left[1 - erf\left(\frac{x}{k}\right)\right] \quad \text{eq. 7}$$

in ToF-SIMS the profiles are measured from the top surface towards the bulk of the materials, eventually crossing the interface between the two materials studied in this case. As a consequence, the interface is not centered in zero but at a depth d, and the diffusion occurs from the interface to the surface (in the "-x" direction) therefore the equation is modified as following:

$$C(x) = C_S\left[1 - erf\left(\frac{d - x}{k}\right)\right] \quad \text{eq. 8}$$

The calculus was made using an in-house developed Python program. The modeling was made from the top of the material till reaching the interface, as the exact distances after the interface are unknown.

The acquisition of a depth profile in ToF-SIMS induces ion mixing at the interface and an increase in roughness [35,36]. In addition, the aluminum surface is still a bit rough (Sa = 18 nm) adding to the uncertainty of the exact location of the interface. These phenomena will be measured along with the diffusion, making it difficult to separate the impact of the diffusion from the other effects. To overcome this issue, two profiles were acquired: one in the weld with possible diffusion and one out of the weld without diffusion occurring. The following assumptions are made: the ion mixing at the interface and the roughness induced by the measurement are the same in and out of the weld. By comparing the two k values in the weld, k_{weld}, and out of the weld, k_{out}, it is possible to define an effective diffusion length, $k_{eff.}$, for a specific ion:

$$k_{eff.} = k_{weld} - k_{out} \quad \text{eq. 9}$$

4. Results and discussion

4.1. Locating the interface

Throughout the years, several methodologies have been used to place the interface between two layers of materials in a ToF-SIMS profile. The simplest methodology is to monitor a specific ion, presenting a drop or an increase of intensity. The interface is placed at 50% of the intensity variation of this specific ion. Another way to set the position of this interface is to select two specific ions, each one characteristic for one of the two materials at the interface. These two ions must each present high intensities. In this case, the interface is placed at the crossing point of the intensity of these two selected ions, normalized to their high intensity plateau value. A few years ago, IONTOF Gmbh proposed a new automatic tool to define the interfaces in their SurfaceLab 7 software. A specific ion must be selected, this tool will then look for the highest variations of intensity and classify them by range. These variations are then modeled using an error function, allowing to derivate them into a Gaussian function. From this Gaussian function two points of 84%/16% are calculated. Of these two points, the one presenting the highest intensity will be selected as the interface location. All these methodologies present an essential disadvantage: the location of the interface depends on the ion selected, thus it is user dependent. This is clearly visible by looking at Table 2, where the sputter times at which the automatic tool of SurfaceLab 7 places the interface for several characteristic aluminum and polyamide-6.6 ions out and in the weld are presented. Depending on the ion selected, the interface will be placed at a very different sputter time of the profile.

Aoyagi et al. [34] used the Shannon or information entropy to get a deeper understanding of the profiles analyzed. They observed that at interfaces the information entropy varies. The information entropy can be seen as the "amount of information" transmitted along the profile, hence describing the complexity of a sample. The higher the entropy the more information is transmitted. Concretely, this means that the more peaks describe a material, the higher the entropy will be, and vice versa. In the extreme case, with only one peak in the spectrum, the entropy would be equal to zero (see part 3.1). When reaching the interfacial region between two materials, the entropy will rise as more peaks are present to describe this specific zone and reach a maximum at the interface, before decreasing while switching to the other material. The information entropies have been calculated out and in the weld and are depicted in Fig. 1 (a) and (b) respectively. In both profiles, the information entropy presents a small plateau at quite high values, followed by an increase up to a maximum and then a strong decrease. As described above, the interface is reached at the maximum of the

Table 2
Sputter time at which SurfaceLab 7 places the interface for several characteristic aluminum and polyamide-6.6 ions out and in the weld.

Ion	Out of the weld	Weld
Al^-	206	156
AlH_2^-	145	84
AlH_5^-	153	99
AlO^-	194	132
$AlOH_2^-$	165	117
AlO_2^-	208	150
AlO_2H^-	173	117
$Al_3O_4^-$	204	151
$Al_7O_{11}^-$	163	111
C_2H^-	237	198
C_2N^-	235	199
$C_3H_2^-$	236	182
CNO^-	250	216
CH_2NO^-	226	129
$C_2H_4NO^-$	210	134
$C_3H_6NO^-$	225	179
$C_5H_9N^-$	217	147
$C_{11}H_{22}NO^-$	230	192
$C_{12}H_{26}N^-$	204	173
$C_{12}H_{26}NO^-$	212	172
Average	**204.7**	**151.9**
Information entropy	**200**	**140**

information entropy. The profilometry experiments gave in both zones a polymer thickness of 110 nm. The maximum is reached at different sputtering times, 200s out of the weld and 140s in the weld. The difference in sputter time at which the interface is reached in and out of the weld, can be explained by the welding process. Indeed, the welding melts the polymer at the interface [11], causing differences in crystallinity, and by extension differences in mechanical and sputtering properties. This structural change could explain why the sputter rate is about 40% higher in the weld than out of it. Nevertheless, this allows to calibrate the depth till the interface. The distance from the interface to the bottom of the sputter crater is unknown. Using Yamamura's formula to calculate the sputter rate of pure compounds [37] a very rough estimate of the depth after the interface could be made. The formula was applied making two crude assumptions: (1) the density of aluminum oxide is nearly the same as pure aluminum, and (2) the sputter rates of aluminum oxide and pure aluminum are also similar. The calculation gives ~13 nm out of the weld and ~14 nm in the weld. As the estimates are very rough, the depth will be indicated until the interface is reached. No depth calibration has been done after.

4.2. Diffusion

In Fig. 2, the information entropies out and in the weld are shown in parallel and depth calibrated. The entropy value in the weld in the polymer zone begins higher than out of the weld, and start to increase earlier to reach nearly the same value at the interface. After it decreases more slowly than out of the weld but reaches the same value in the end. As the entropy is already different at the beginning, the polymer is modified due to the welding. In addition, the sputter time at which the interface is reached is also different, as described above (see Table 2). The welding brings the polymer to melt in the weld area [11], which will modify its crystallinity, hence its mechanical properties in the weld. The welding also induces chemical bonding at the interface [29–31]. These two phenomena help to understand part of the differences between the two zones, but a diffusion phenomenon also plays a decisive role in explaining these differences.

Fig. 3(a) depicts the depth calibrated profiles of several characteristic ions out and in the weld of the ions Al^- and O_2^-, while Fig. 3 (b)depicts AlO^- and AlO_2^-. The ion O_2^- out of the weld begins at a low value reaches a low intensity plateau and then its intensity increases around 60 nm and reaches a maximum value around the interface and then its intensity decreases. In the weld for the same ion, the intensity increases till reaching a maximum before the interface around 80 nm and then decreases again. The welding loads the polymer with oxygen species, diffusing from the aluminum oxide. The profiles of more specific aluminum or aluminum oxide ions (Al^-, AlO^- and AlO_2^-) show similar trends. Out of the weld, the intensity of these three ions goes from a low intensity value to a high intensity plateau when reaching the interface. The same ions in the weld, begin at a higher level of intensity, and their intensity increase till reaching a high intensity plateau at the interface, nearly at the same level as out of the weld. The welding induces differences, the intensity increasing directly, without low intensity plateau. These differences are signatures for diffusion. Fig. 3 (c) depicts the profiles in and out of the weld for two characteristic ions of the polyamide-6.6 (CNO^-, and $C_2H_4NO^-$). These ions present a high

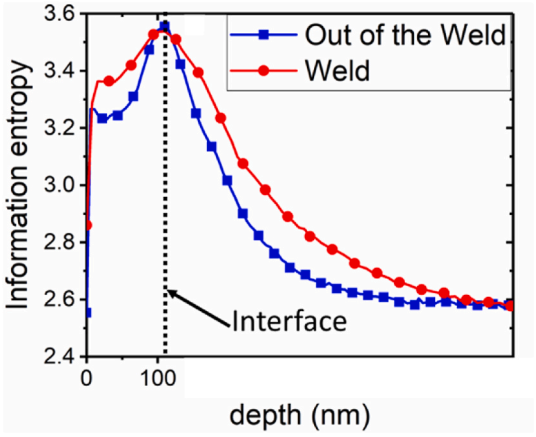

Fig. 2. Information entropy versus depth out and in the weld (see eq. (1)).

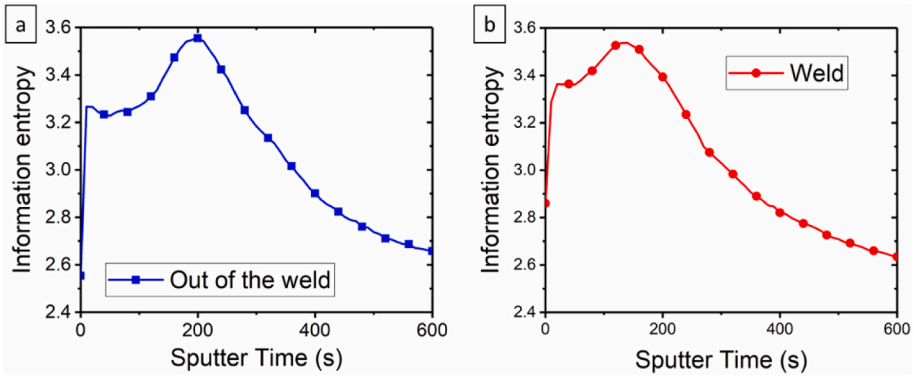

Fig. 1. Information entropy in sputter time (a) out and (b) in the weld (see eq. (1)).

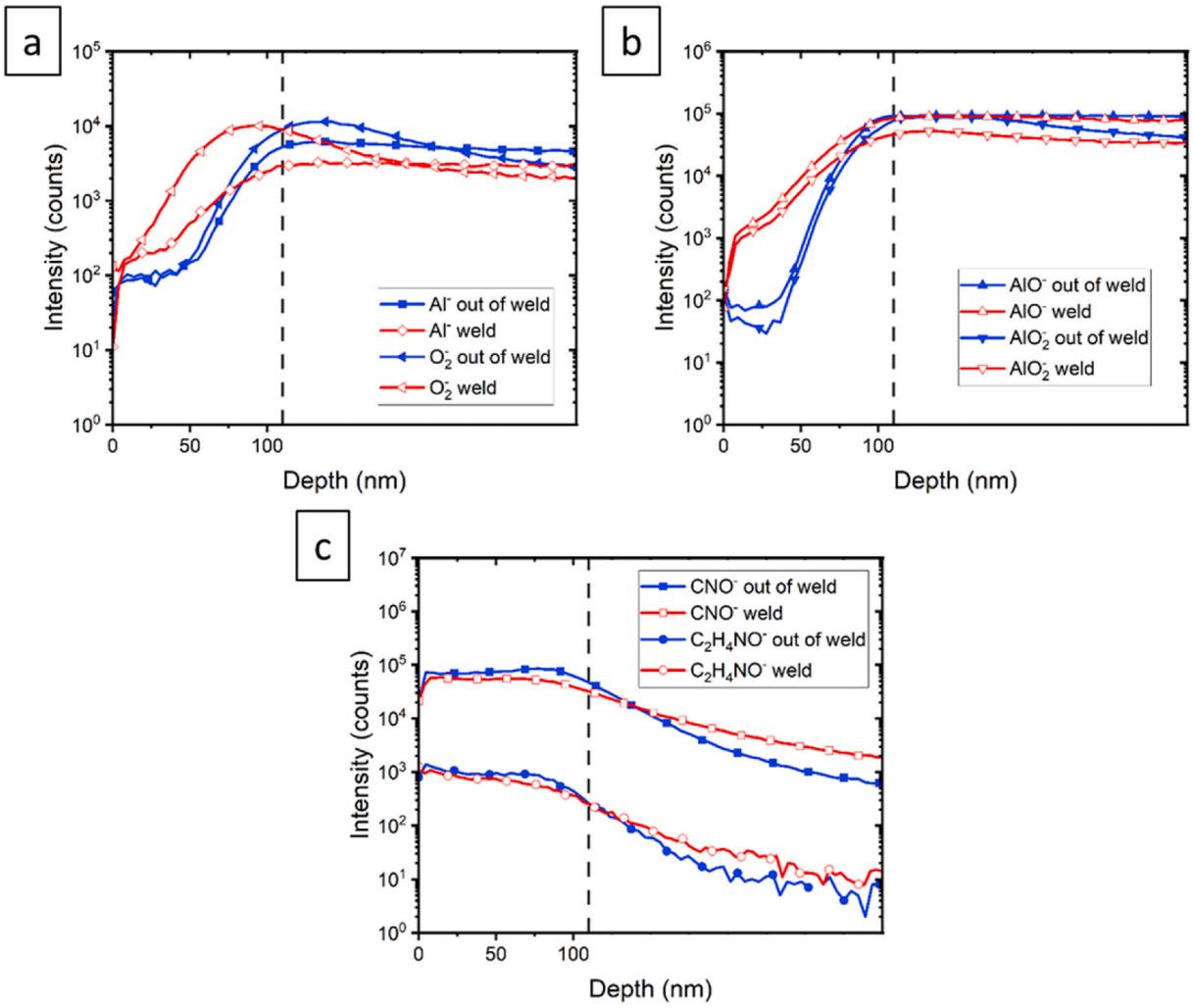

Fig. 3. Depth profiles in and out of the weld (a) for Al^- and O_2^-, (b) for AlO^- and AlO_2^- and (c) for CNO^- and $C_2H_4NO^-$. As the depth after the interface is not calibrated, the depth scale stops at the interface at 110 nm.

intensity plateau at the beginning of the profile, as they are characteristic of the polyamide-6.6. At the interface their intensity begins to drop, but not at the same rate out and in the weld. The difference seems quite important, but the scale is not adapted after the interface. As described above, a rough estimate of the distance between the interface and the end of the profiles gives 13 nm out of the weld and 14 nm in the weld. Nonetheless, the difference of intensity drop is systematical, and could be explained by the chemical bonds forming at the interface during the welding [29–31]. The polymer is more intimately bonded to the aluminum surface, making it more difficult to remove during the sputtering.

To calculate the diffusion length, the Second Fick law was applied as described in part 3.2. The modeling was done till the interface was reached, as the distances after the interface are not exactly known. The modeling was made on three characteristic aluminum (Al^-, AlO^-, AlO_2^-) ions out and in the weld, as presented in Fig. 4. The values of the different curves are presented in Table 3. Looking at the curves, the fits are quite good for Al^- and AlO_2^- (Fig. 4 (a) and (c) respectively), which is supported by their high R^2 (>0.990). When comparing the fits out and in the weld, it is all the more visible that the intensity increases sooner and reaches the maximum of intensity around the interface in the weld. Out of the weld, the maximum of intensity is reached after the interface. This underlines more clearly the diffusion phenomenon happening due to the laser welding. AlO^- presents a less good fitting, especially in the weld also reflected by the lower values of R^2. Looking at the signal of this ion, it begins to saturate near the interface. This explains why the signal reaches a plateau before the interface. The saturation explains the bad fit when all the data are fed to the fitting algorithm.

The effective diffusion lengths of the three studied ions were calculated as described in part 2.8 and are presented in Table 4. The results for Al^- and AlO_2^- are very similar, while AlO^- is slightly higher but in the same order of magnitude. This discrepancy is explained by the saturation of the AlO^- signal both out and in the weld leading to a relatively poor fit. The effective diffusion length calculated here are significantly below the size of the melted area and the heat affected zone as described and characterized by Schricker et al. [38], which reach a few micrometers for thick polyamide-6.6. So, the diffusion occurs in the molten area. The authors observe a difference in the mechanical properties of the polymer depending on the welding parameters, but as they study the effects on the micrometer scale, the impact of diffusion occurring in the nanoscale is completely negligible and could not be characterized yet.

5. Conclusions

This work showed successfully that the Shannon or information entropy can be used to place correctly an interface in a ToF-SIMS depth profile with a greater accuracy than other methods used so far in simple samples. This allowed to characterize and show the existence of a diffusion phenomenon of aluminum in polyamide during the laser welding of an aluminum-polyamide assembly. The effective diffusion

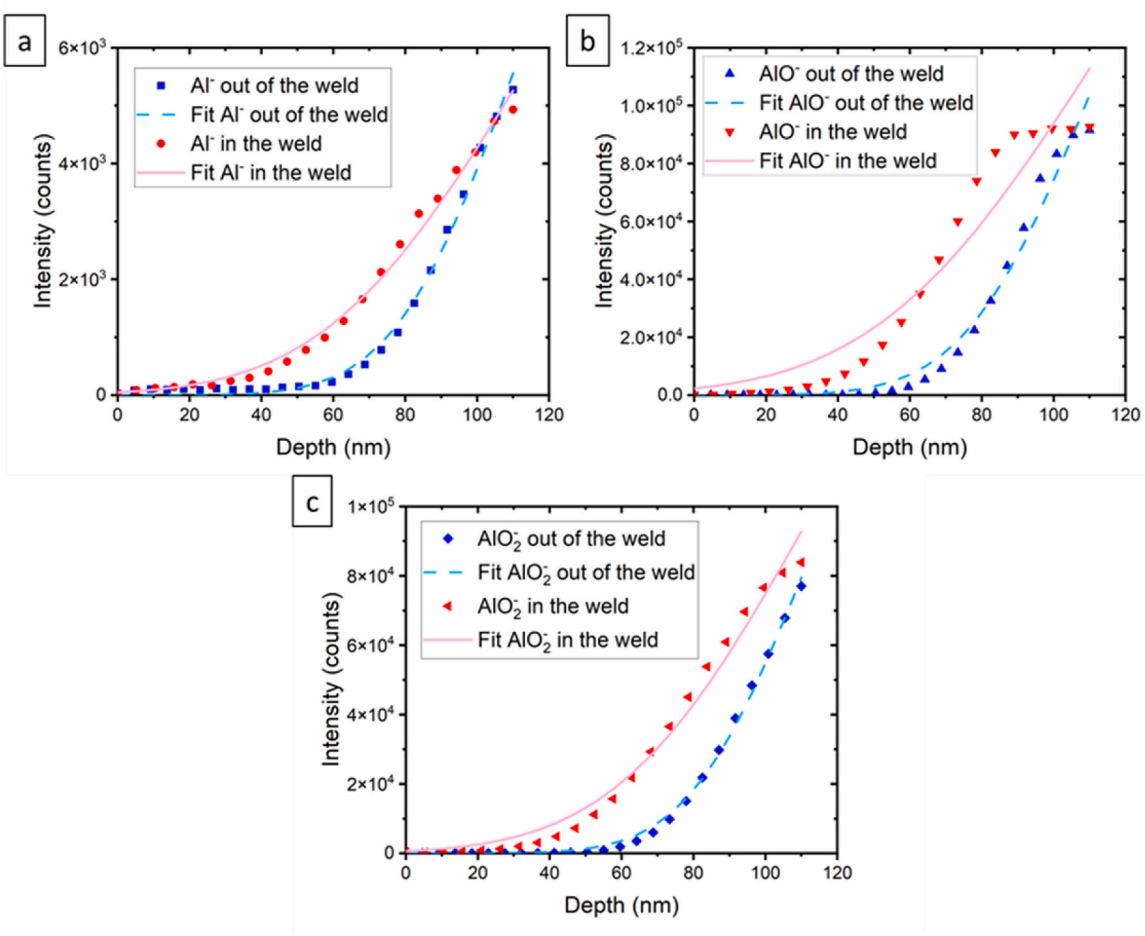

Fig. 4. Comparison of the experimental data and the fits obtained out and in the weld (a) for Al^-, (b) for AlO^- and (c) for AlO_2^- (see eq. (8)).

Table 3
Fitting parameters in and out of the weld for Al^-, AlO^-, and AlO_2^- (see eq. (8)).

	C_S	d	R^2
Al- out	5559.2	37.0	0.995
Al- weld	5258.6	59.6	0.993
AlO- out	103750.5	38.8	0.982
AlO- weld	112800.7	67.1	0.932
AlO2- out	79482.9	35.3	0.998
AlO2- weld	92780.9	57.7	0.986

Table 4
Diffusion length calculated for each ion by subtracting the k parameter in and out of the weld (see eq. (9)).

	Al-	AlO-	AlO2-
Distance out	37.0	38.8	35.3
Distance weld	59.6	67.1	57.7
Effective diffusion length (nm)	**22.6**	**28.3**	**22.4**

distance is about 20–25 nm for the monoatomic Al^-, AlO^- and AlO_2^- species. The impact of this diffusion phenomenon on the adhesion strength or the materials mechanical properties could not be assessed here, but should be in the future to gain a deeper understanding on laser welding.

Declaration of competing interest

The authors declare that they have no known competing financial interests or personal relationships that could have appeared to influence the work reported in this paper.

Acknowledgements

The authors would like to thank the DGO6 of the Walloon region and the FNR of Luxembourg for financing the M-Era.Net project named LaserSTAMP, frame of this study. The ToF-SIMS were performed using the equipment and the materials of the SIAM platform of the University of Namur.

Appendix A. Supplementary data

Supplementary data to this article can be found online at https://doi.org/10.1016/j.jmrt.2024.11.092.

References

[1] Speck JA. Mechanical fastening, joining, and assembly. second ed. 2015. https://doi.org/10.1201/9781351228640.
[2] Skeist I. Handbook of adhesives. third ed. London: Springer Science & Business Media; 2012.
[3] Allen KW. Adhesion and adhesives – some fundamentals. Stud Conserv 1984;29:5–12. https://doi.org/10.1179/sic.1984.29.Supplement-1.5.
[4] Ageorges C, Ye L. State of the art in fusion bonding of polymer composites. In: Ageorges C, editor. Fusion bonding of polymer composites. London: Spinger; 2002. p. 7–64.
[5] Yousefpour A, Hojjati M, Immarigeon JP. Fusion bonding/welding of thermoplastic composites. J Thermoplast Compos Mater 2004;17:303–41. https://doi.org/10.1177/0892705704045187.

[6] da Costa AP, Botelho EC, Costa ML, Narita NE, Tarpani JR. A review of welding technologies for thermoplastic composites in aerospace applications. J Aero Technol Manag 2012;4:255–65. https://doi.org/10.5028/jatm.2012.04033912.
[7] Amancio-Filho ST, Dos Santos JF. Joining of polymers and polymer-metal hybrid structures: recent developments and trends. Polym Eng Sci 2009;49:1461–76. https://doi.org/10.1002/pen.21424.
[8] Katayama S. Fundamentals and details of laser welding. Osaka: Springer; 2020.
[9] Bardon J, Del Frari D, Al-Sayyad A, Hirchenhahn P, Houssiau L, Plapper P. Laser welding of polyamide-6.6 and aluminium. Adhesion'19; 2019.
[10] Al-Sayyad A, Bardon J, Hirchenhahn P, Santos K, Houssiau L, Plapper P. Aluminum pretreatment by a laser ablation process: influence of processing parameters on the joint strength of laser welded aluminum - polyamide assemblies. Procedia CIRP 2018;74:495–9. https://doi.org/10.1016/j.procir.2018.08.136.
[11] Lamberti C, Solchenbach T, Plapper P, Possart W. Laser assisted joining of hybrid polyamide-aluminum structures. Phys Procedia 2014;56:845–53. https://doi.org/10.1016/j.phpro.2014.08.103.
[12] Katayama S, Kawahito Y. Laser direct joining of metal and plastic. Scripta Mater 2008;59:1247–50. https://doi.org/10.1016/j.scriptamat.2008.08.026.
[13] Kumar N, Kumar N, Bandyopadhyay A. A state-of-the-art review of laser welding of polymers - Part I: welding parameters. Weld J 2021;100:221–8. https://doi.org/10.29391/2021.100.019.
[14] Bergmann JP, Stambke M. Potential of laser-manufactured polymer-metal hybrid joints. Phys Procedia 2012;39:84–91. https://doi.org/10.1016/j.phpro.2012.10.017.
[15] Roesner A, Scheik S, Olowinsky A, Gillner A, Reisgen U, Schleser M. Laser assisted joining of plastic metal hybrids. Phys Procedia 2011;12:370–7. https://doi.org/10.1016/j.phpro.2011.03.146.
[16] Wahba M, Kawahito Y, Katayama S. Laser direct joining of AZ91D thixomolded Mg alloy and amorphous polyethylene terephthalate. J Mater Process Technol 2011;211:1166–74. https://doi.org/10.1016/j.jmatprotec.2011.01.021.
[17] Yusof F, Mutoh Y, Miyashita Y. Effect of pre-oxidized CuO layer in joining between polyethylene terephalate (PET) and copper (Cu) by using pulsed Nd:YAG laser. Adv Mater Res 2010;129–131:714–8. https://dx.doi.org/10.4028/www.scientific.net/AMR.129-131.714.
[18] Georgiev GL, Sultana T, Baird RJ, Auner G, Newaz G, Patwa R, et al. Laser bonding and characterization of Kapton® FN/Ti and Teflon® FEP/Ti systems. J Mater Sci 2009;44:882–8. https://doi.org/10.1007/s10853-008-3187-8.
[19] Wang X, Li P, Xu Z, Song X, Liu H. Laser transmission joint between PET and titanium for biomedical application. J Mater Process Technol 2010;210:1767–71. https://doi.org/10.1016/j.jmatprotec.2010.06.007.
[20] Arai S, Kawahito Y, Katayama S. Effect of surface modification on laser direct joining of cyclic olefin polymer and stainless steel. Mater Des 2014;59:448–53. https://doi.org/10.1016/j.matdes.2014.03.018.
[21] Al-sayyad A, Bardon J, Hirchenhahn P, Vaud R. Influence of aluminum laser ablation on interfacial. Coatings 2019;9:768.
[22] McBain W, Hopkins DG. ON adhesives and adhesive action. J Phys Chem 1925;29:188–204.
[23] Sharpe LH, Schonhorn H. Surface energetics, adhesion, and adhesive joints. Contact Angle, Wettability, and Adhesion 1964;43(UTC):189–201.
[24] Voyutskii SS. Adhesion and autohesion of polymers. Adhes Age 1962;5.
[25] Voyutskii SS, Vakula VL. The role of diffusion phenomena in polymer-to-polymer adhesion. J Appl Polym Sci 1963;7:475–91. https://doi.org/10.1002/app.1963.070070207.
[26] Derjaguin BV, Smilga VP. Electronic theory of adhesion. J Appl Phys 1967;38:4609–16. https://doi.org/10.1063/1.1709192.
[27] Xu R, Xie Y, Li R, Zhang J, Zhou T. Direct bonding of polymer and metal with an ultrahigh strength: laser treatment and mechanical interlocking. https://doi.org/10.1002/adem.202001288; 2021.
[28] Georgiev GL, Baird RJ, McCullen EF, Newaz G, Auner G, Patwa R, et al. Chemical bond formation during laser bonding of Teflon ® FEP and titanium. Appl Surf Sci 2009;255:7078–83. https://doi.org/10.1016/j.apsusc.2009.03.046.
[29] Hirchenhahn P, Al Sayyad A, Bardon J, Felten A, Plapper P, Houssiau L. Highlighting chemical bonding between nylon-6.6 and the native oxide from an aluminum sheet assembled by laser welding. ACS Appl Polym Mater 2020;2:2517–27. https://doi.org/10.1021/acsapm.0c00015.
[30] Hirchenhahn P, Al-Sayyad A, Bardon J, Plapper P, Houssiau L. Binding mechanisms between laser-welded polyamide-6.6 and native aluminum oxide. ACS Omega 2021;6:33482–97. https://doi.org/10.1021/acsomega.1c04264.
[31] Hirchenhahn P, Al Sayyad A, Bardon J, Plapper P, Houssiau L. Probing the reaction mechanism between a laser welded polyamide thin film and titanium with XPS and ToF-SIMS. Talanta 2022;247:123539. https://doi.org/10.1016/j.talanta.2022.123539.
[32] Baldan A. Adhesion phenomena in bonded joints. Int J Adhesion Adhes 2012;38:95–116. https://doi.org/10.1016/j.ijadhadh.2012.04.007.
[33] Shannon CEA. Mathematical theory of communication. 1948.
[34] Aoyagi S, Mizomichi K, Kamochi K, Miisho A. Interpretation of TOF-SIMS data based on information entropy of spectra. Surf Interface Anal 2022;54:356–62. https://doi.org/10.1002/sia.7047.
[35] Vickerman JC, Briggs D. TOF-SIMS: materials analysis by mass spectrometry. second ed. IM Publications; 2013.
[36] Noël C, Busby Y, Mine N, Houssiau L. ToF-SIMS depth profiling of organic delta layers with low-energy cesium ions: depth resolution assessment. J Am Soc Mass Spectrom 2019;30:1537–44. https://doi.org/10.1007/s13361-019-02224-4.
[37] Matsunami N, Yamamura Y, Itikawa Y, Noriaki Itoh, Kazumata W, Miyagawa S, et al. Energy dependence of the ION-induced sputtering yields of monatomic solids. AtOmlo Data and Nudenr Data Tables 1984;31.
[38] Schricker K, Stambke M, Bergmann JP. Experimental investigations and modeling of the melting layer in polymer-metal hybrid structures. Weld World 2015;59:407–12. https://doi.org/10.1007/s40194-014-0213-0.